A model for describing and predicting the creep strain of rocks from the primary to tertiary stage

Ruofan Wang[1,*], Li Li[1,2], Richard Simon[1,2]

[1]Research Institute on Mines and Environment (RIME UQAT-Polytechnique)

[2]Department of Civil, Geological and Mining Engineering
École Polytechnique de Montréal
C.P. 6079 succursale Centre-ville
Montréal, Québec, Canada H3C 3A7

[*]Author of correspondence. Tel: 1-514-677-2962; email: ruofan.wang@polymtl.ca

Manuscript IJRMMS-2018-937-R1 resubmitted to *International Journal of Rock Mechanics and Mining Sciences*

Submitted: October 2018
Comment received: December 2018
Revised version resubmitted: March 2019
Comment received on revised version: April 2019
Re-revised version resubmitted: June 2019

A model for describing and predicting the creep strain of rocks from the primary to tertiary stage

Ruofan Wang*, Li Li, Richard Simon

Abstract: Rocks under applied stresses can exhibit more or less degree of creep. Over the years, a large number of creep models have been proposed for rocks. However, few models account for friction angle and time to failure. In most cases, curve fitting technique is applied to all of the available experimental results to obtain the required model parameters. The ability of the calibrated model (i.e. the model with the obtained model parameters) to predict the rheological behavior under untested stress conditions remains unknown. In this paper, a new model, called ubiquitous-corrosion-Coulomb (UCC) creep model, is proposed. Distinction is made between reversible and irreversible creep strains. Subcritical crack growth is related to the irreversible creep strain and delayed failure of rocks. The effect of friction angle and confining stresses on the rate of irreversible creep strain and time to failure has been considered. With the UCC model, the failure plane in creep tests making an angle of $45°-\phi/2$ with the major principal stress σ_1 is explained by the fact that among the numerous micro cracks, the cracks along this orientation are the first ones becoming instable. To test the capability of the UCC creep model against experimental results available in the literature, the required model parameters are first obtained by applying the curve-fitting technique on a part of the available experimental results. The predictability of the calibrated model is then tested against another part of the available experimental results, which are not used in the previous curve-fitting process. The results showed that the proposed UCC creep model can be used to describe and predict the creep strain and time to failure of rocks.

Key-words: rock mechanics; rheological model; creep; time to failure; description; prediction

* Corresponding author. Tel: 1-514-677-2962; email: ruofan.wang@polymtl.ca

1. Introduction

When a rock is submitted to a sufficiently high (but below its peak strength) and constant load, it may deform continuously with time. This strain evolution is well known as rheological behavior or creep.[1] Most rocks can exhibit a more or less degree of creep. Soft rocks usually demonstrate more pronounced creep phenomenon than hard rocks.[2] Under high stress or thermal conditions, hard rocks can also show significant rheological behavior.[3, 4] An excessive deformation due to creep can affect the designed function of rock infrastructures and increase the cost of rehabilitation. This is the case when the project is in a soft or weak rock, in a deep mine, or for radioactive waste storage.[5-7] In extreme cases, structure instability can take place.[8] It is thus important to well understand the rheological behavior and characterize the creep deformation around a rock infrastructure. This requires a model that is able to describe and further predict the creep process of rock under different stress conditions.

Figure 1 schematically shows the rheological behavior of rock. Upon an instantaneous loading, one first sees an instantaneous elastic deformation. After then, the rock can continue to deform with time while the load is maintained constant. Creep takes place and generally exhibits three stages from the start to the failure of the rock: primary (or transient creep) stage, secondary (or steady creep) stage and tertiary (or accelerating) stage.[9-11]

The primary stage is featured by a creep strain rate very high at the beginning and progressively decreased with time. The secondary stage is characterized by a creep strain rate almost constant with time. In the tertiary stage, the creep strain rate accelerates and usually ends by the failure of the rock. The total strain, ε_t, can then be calculated as the sum of the strains at different stages:

$$\varepsilon_t = \varepsilon_e + \varepsilon_{pc} + \varepsilon_{sc} + \varepsilon_{tc} \quad (1)$$

where ε_e denotes the instantaneous elastic strain; ε_{pc}, ε_{sc} and ε_{tc} are the creep strains of the primary, secondary and tertiary creep stages, respectively.

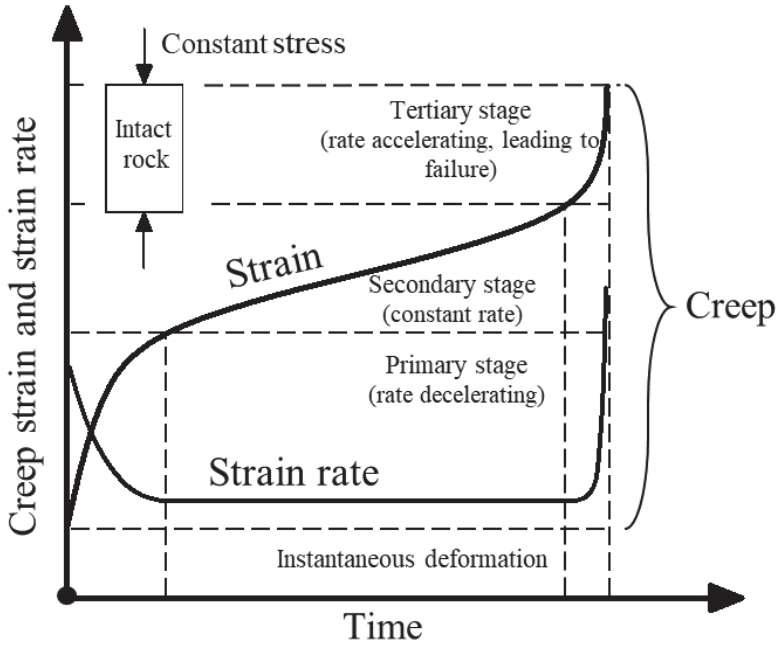

Figure 1. A schematic presentation of rheological behavior of rock (adapted from Goodman[9])

A number of studies have been reported on the creep behavior of rocks. Ngwenya et al.[12] and Amitrano et al.[10] have shown that the strain rate of the secondary creep stage increases as the deviatoric stress increases and decreases as the confining pressure increases. Lajtai et al.[13] and Cristescu et al.[2] reported that the tertiary creep stage only occurs when the applied stress exceeds a certain critical value, known as the long-term strength of the rock. The time to failure decreases as the applied stress and steady-state rate increase.[14-16]

During the primary and secondary creep stages, acoustic emissions (AE) took place through almost the whole sample, indicating the cracking or/and crack propagation during the two creep stages. These results can explain the occurrence of reversible and irreversible strains when the rocks were submitted to loading and unloading conditions.[17-19] During the tertiary creep stage, the AE coalesce around a plane and end by the formation of a failure plane, as shown in Figure 2a.

Figure 2b shows the typical failures of a brittle rock in creep and conventional compressive tests, respectively.[20, 21] The high similarity between the shapes of failure indicates that the failure of the rock is controlled by shear in the creep tests as in the conventional compressive tests.

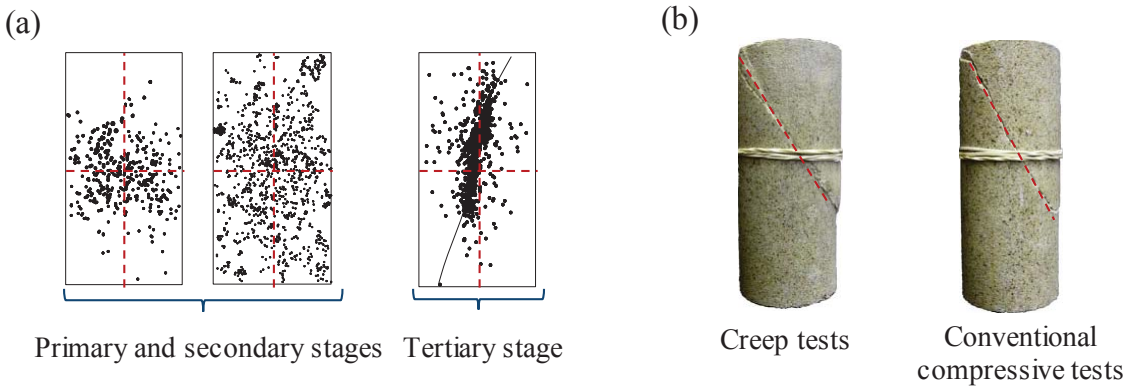

Figure 2. (a) AE observed during the three stages of a creep test (taken from Hirata et al.[22] for the primary stage and Lei et al.[23] for the secondary and tertiary stages); (b) typical failures of a rock submitted to creep and conventional compression tests (taken from Brantut et al.[20])

Over the year, a number of models have been proposed to describe the creep behavior of rocks. They can generally be divided into empirical [24-30] and rheological model-based[16, 31-36] formulations. The empirical models for rocks were mostly initially proposed to describe the creep behavior of metals.[37-39] The formulations were established based on observed time-creep strain data to phenomenally describe the strain evolution. The empirical models are simple, but the model parameters do not have any physical meaning. Friction angle is neglected. Stresses are absent or only deviatoric stress is involved. These formulations can only be used to describe the obtained experimental data. They cannot be applied to predict the creep behavior of rocks under different stress states.

The rheological models were developed to reflect the mechanical behavior of rocks submitted to mechanical solicitations. Elastic spring, dashpot, and plastic slider are the commonly used elements in the classic and fundamental one-dimensional rheological models to simulate the elasticity, viscosity and plasticity of materials.[9, 40] The models are able to describe the creep strain of the primary or/and secondary creep stages, but fail to describe the irreversible creep strains. This is the case for the Maxwell, Kelvin-Voigt, generalized Kelvin-Voigt and Burgers creep models.[40] When a plastic slider element is incorporated, the models can describe the plasticity, irreversible creep strains and triggering of the tertiary creep stage, but fail to characterize the time to failure of

the tertiary creep stage. This is the case of the CVISC[41] and Bingham creep models.[11] To note that the Bingham creep model stipulates that the creep strain is possible only when the applied load exceeds a certain threshold. This may not reflect the reality as many short and long-term creep tests on rocks showed that creep can take place even in very low applied stresses.[19, 42-44] Similar to the empirical formulations, the fundamental rheological models omit the friction angle and confining stress. This is a typical feature of frictionless materials like metals, not that of geomaterials like rocks. It does not correspond to the experimental observations on rocks.[12, 20]

Maranini and Yamaguchi[45] proposed an elastic-visco-plastic model by considering mean stress dependency of shear and bulk modulus. Friction angle is neglected. Perzyna[46] proposed a theory of overstress, in which the material has an elasto-visco behavior when the stress point is below the elastic surface. When the applied stress point exceeds the elastic surface and below the yield surface, the rock exhibits an elasto-visco-plastic behavior. The confining pressure dependency of creep strain was not considered. The model cannot be used to describe or predict the tertiary creep stage of rocks.

Yahya et al.[47] proposed an internal state variable elasto-visco-plastic model based on a visco-plastic model proposed by Aubertin et al.[48] to describe the stress-strain relationship under testing conditions of constant strain rate and time-strain relationship under constant stress (creep) or constant strain (relaxation) test conditions. Shao et al.[49] developed a damage evolution model by associating the creep deformation to the propagation of sub-critical micro cracks. These models are much more powerful to describe the creep behavior of rocks under different conditions. However, these models involve a large number of model parameters and require a large quantity of tests (ideally under divers stress conditions). For most cases, all of the available experimental results have to be used to obtain the required model parameters. The good agreements between the model and experimental results are of descriptive nature, not predictive nature.[19, 21, 50-52] In addition, the failure plane making an angle of $45°-\phi/2$ with the major principal stress σ_1 in creep tests has not been explained by previous studies[49, 53-56].

In this study, a new creep model is proposed to describe and predict the creep strains of the

three creep stages and time to failure for rocks under different stress states. Distinction is made between reversible and irreversible creep strains. The irreversible creep strain and delayed failure are associated with the growth of micro cracks. For a given rock with some available experimental results, the required model parameters are first obtained by applying the curve-fitting technique on a part of the available experimental results. The calibrated model (i.e. the model with the obtained model parameters) is then applied to the other part of the available experimental results (not participating in the previous curve-fitting process) to test the predictability of the calibrated model.

2. A new creep model

In the previous section, it has been shown that the creep strain can be divided into reversible and irreversible parts. Friction angle, deviatoric stress and confining pressure should be involved in the models to reflect the frictional feature of geomaterials. More work is also needed to better describe the strain of the tertiary accelerating creep stage. Here, a new creep model, called UCC (standing for Ubiquitous-Corrosion-Coulomb) creep model is proposed.

The Coulomb criteria is involved in the new model for the clear physical meaning of the material parameters (cohesion and friction angle) and its simplicity. Regarding the stress corrosion, its presence is reflected by the AE activities recorded throughout tested samples (Figure 2). The growth of micro cracks is considered as the origin of the AE activities, change in the internal stresses and source for the irreversible creep strain. It is a mechanism responsible for the creep behavior under a stress lower than the peak strength but higher than a threshold.[57, 58] Its process can be affected by several aspects, including chemical reaction, stress states, mineral composition and initial geometry of grains.[59, 60] In this study, a simple geometry of cracks is considered while the creep strain and time to failure associated with the crack propagation will be analyzed.

Figure 3 shows a schematic presentation of the UCC creep model. The model is composed of a generalized Kelvin-Voigt model, a Newton dashpot and a Ubiquitous-Corrosion (UC) element. The generalized Kelvin-Voigt model is responsible for the instantaneous deformation and creep strain of the primary stage. The Newton dashpot is used to describe the reversible strain of the secondary creep stage. The UC element is introduced to represent the irreversible strain of the

secondary creep stage. It is also responsible for the strain of the tertiary creep stage. The total axial strain of the UCC creep model can still be written as Eq. 1.

In the following subsections, the formulation and development of the UCC model will be shown by considering conventional triaxial compression test conditions (i.e. $\sigma_1 \geq \sigma_2 = \sigma_3$; where σ_1, σ_2 and σ_3 are the major, intermediate and minor principle stresses, respectively).

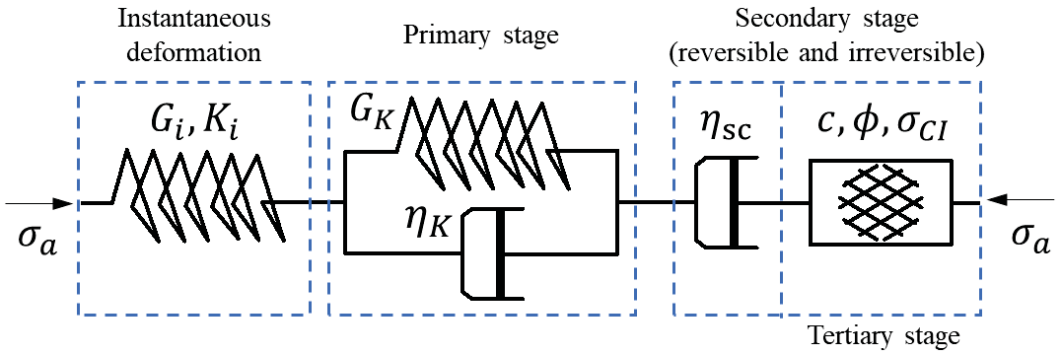

Figure 3. A schematic presentation of the UCC creep model

2.1 Instantaneous deformation

As discussed above, the instantaneous deformation of rocks under a stress below its short-term strength can be represented by a spring as shown in Figure 3. Possible irreversible instantaneous deformation resulted from the closure of initial cracks or pores is not considered by this element.

According to the Hooke's law, the total axial elastic strain ε_1^e in conventional triaxial compression tests can be expressed as follows:

$$\varepsilon_1^e = \frac{\sigma_1 + 2\sigma_3}{9K_e} + \frac{\sigma_1 - \sigma_3}{3G_e} \tag{2}$$

where K_e and G_e are bulk and shear modulus, respectively. The axial elastic strain ε_1^e associated with the confining pressure (σ_3) is expressed as follows:

$$\varepsilon_1^e = \frac{\sigma_3}{3K_e} \tag{3}$$

The axial instantaneous strain ε_e caused by the applied deviatoric stress σ_a (= $\sigma_1 - \sigma_3$) can

then be obtained by subtracting Eq. 3 from Eq. 2 as follows:

$$\varepsilon_e = \frac{\sigma_1 - \sigma_3}{9K_e} + \frac{\sigma_1 - \sigma_3}{3G_e} \tag{4}$$

2.2 Primary creep stage

The Kelvin-Voigt visco-elastic body is used here to reflect the primary creep stage as shown in Figure 3. The axial creep strain ε_{pc} under a conventional triaxial compression test condition is given as:

$$\varepsilon_{pc} = \frac{\sigma_1 - \sigma_3}{3G_K}\left[1 - exp\left(-\frac{G_K \cdot t}{\eta_K}\right)\right] \tag{5}$$

where G_K and η_K are the shear modulus and viscosity coefficient of the Kelvin-Voigt body, respectively.

2.3 Secondary creep stage

As shown in Figure 3, the Newton dashpot and UC element are combined for simulating the creep strain of the secondary creep stage.

The Newton dashpot is characterized by the viscosity coefficient η_{sc}, while the UC element by the cohesion c, internal frictional angle ϕ and crack initiation stress σ_{CI} (under compression conditions). The secondary creep strain rate $\dot{\varepsilon}_{sc}$ is decomposed into rates of reversible ($\dot{\varepsilon}_{sc}^{r}$) and irreversible ($\dot{\varepsilon}_{sc}^{ir}$) strains. The rate of reversible creep strain $\dot{\varepsilon}_{sc}^{r}$ is contributed by the visco-elasticity.[61] Therefore, it can be represented by Newton dashpot. Regarding the rate of irreversible strain $\dot{\varepsilon}_{sc}^{ir}$, it is related to the UC element. The secondary creep strain rate $\dot{\varepsilon}_{sc}$ can then be expressed as follows:

$$\dot{\varepsilon}_{sc} = \dot{\varepsilon}_{sc}^{r} + \dot{\varepsilon}_{sc}^{ir} \tag{6}$$

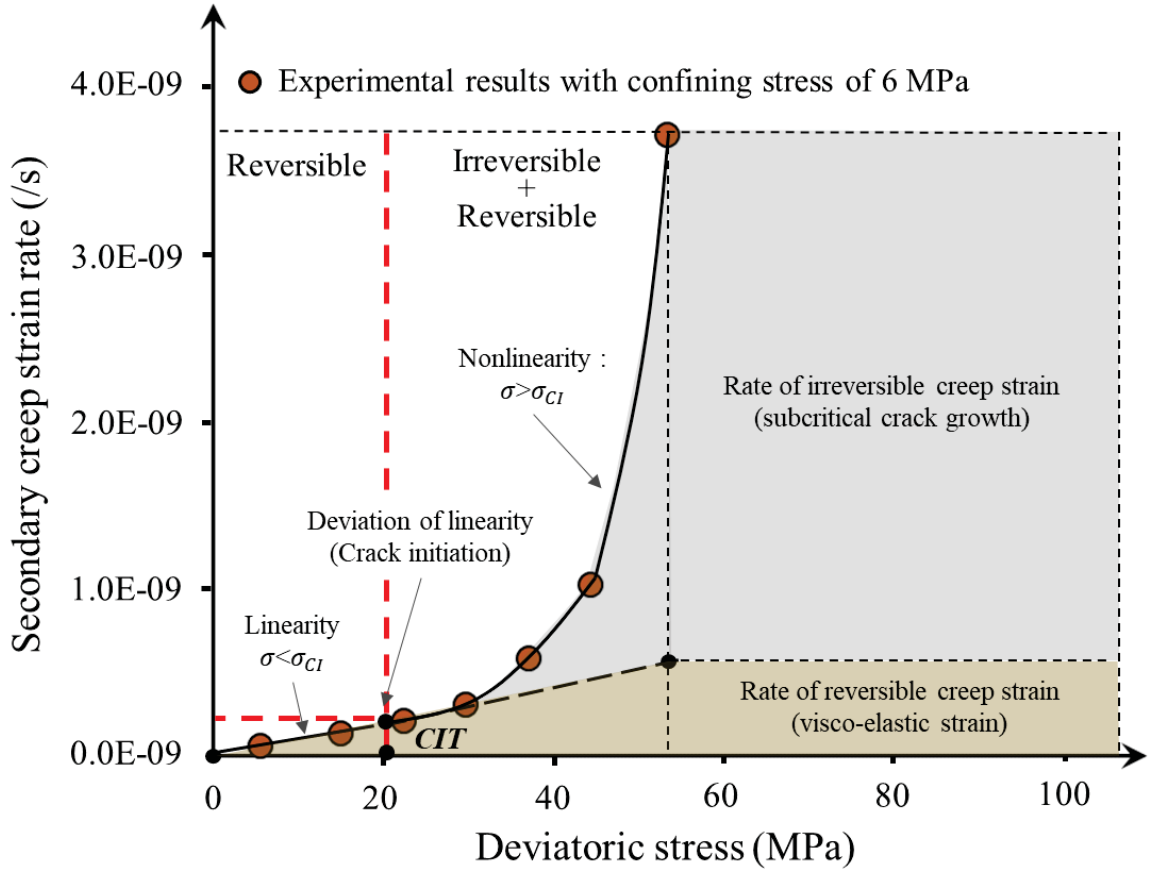

Figure 4. Variation of the creep strain rates during the secondary stage as a function of the deviatoric stress (experimental results taken from Zhao et al.[19])

As previously mentioned, irreversible strain associated with the subcritical crack growth has been illustrated by the AE activities observed during the creep tests until the failure of the rock.[12, 20, 23] However, crack propagation can only take place when the applied stress exceeds a threshold value, known as crack initiation threshold (CIT).[58, 62-64] When the applied stress is below the CIT, no crack growth takes place. Creep occurs nevertheless.[19, 42-44] The rock has a visco-elastic behavior and the creep strain is reversible.[61] The rate of reversible creep is linearly related to the deviatoric stress through viscosity coefficient, as shown in Figure 4. When the applied stress is higher than the CIT, irreversible creep strain occurs and the creep strain is the result of reversible and irreversible creep strains. The relationship between the creep strain rate and deviatoric stress becomes nonlinear, as shown in Figure 4. This is the physical basis of the UCC creep model for the creep strain of the secondary creep stage.

The value of the CIT depends on the type and mineralogy of rocks. It is determined as the start of deviation of the axial stress-radial strain curve from the linearity, start of acoustic emission, or start of dilation. Table 1 presents a summary of the CIT for different rocks under uniaxial and triaxial compression test conditions. Its value generally varies from 0.3 to 0.7 of the short-term peak strength. In the absence of CIT measurement, a value equaling to 0.5 times the short-term strength is commonly suggested.[13, 62]

Table 1. A summary of the CIT values for different rocks under compressive conditions.

Rocks	Ratios of CIT over short-term strength[§]	Compression conditions	References
Granite; marble; aplite	30 to 70%	Triaxial	Brace et al.[65]
Argillaceous quartzite	40 to 60%	Triaxial	Hallbauer et al.[66]
Granite and anorthosite	≤ 60%	Uniaxial	Lajtai and Schmidtke[13]
Igneous; metamorphic; sedimentary	40 to 60%	Uniaxial	Aydan et al.[67]
Lac du Bonnet granite	~30%	Triaxial	Martin[68]
Granitoid rocks	35 to 50%	Uniaxial	Diederichs et al.[63]
Jurassic limestone; Cobourg limestone	~40%	Uniaxial	Paraskevopoulou et al.[16]
Low porosity rocks	30 to 70%	Uniaxial	Li et al.[64]

Note: The CIT and short-term strength are all in deviatoric stresses.

2.3.1 Rate of the reversible creep strain

As rock under a stress state below the CIT is visco-elastic and the creep strain is reversible, the Newton dashpot with viscosity coefficient η_{sc} can be applied to describe the rate of the reversible creep strain during the secondary creep stage as shown in Figure 3. Viscosity coefficient is independent on confining pressure.[40] The rate of reversible creep strain can then be expressed as follows[40, 41]:

$$\dot{\varepsilon}_{sc}^{r} = \frac{\sigma_1 - \sigma_3}{3\eta_{sc}} \tag{7}$$

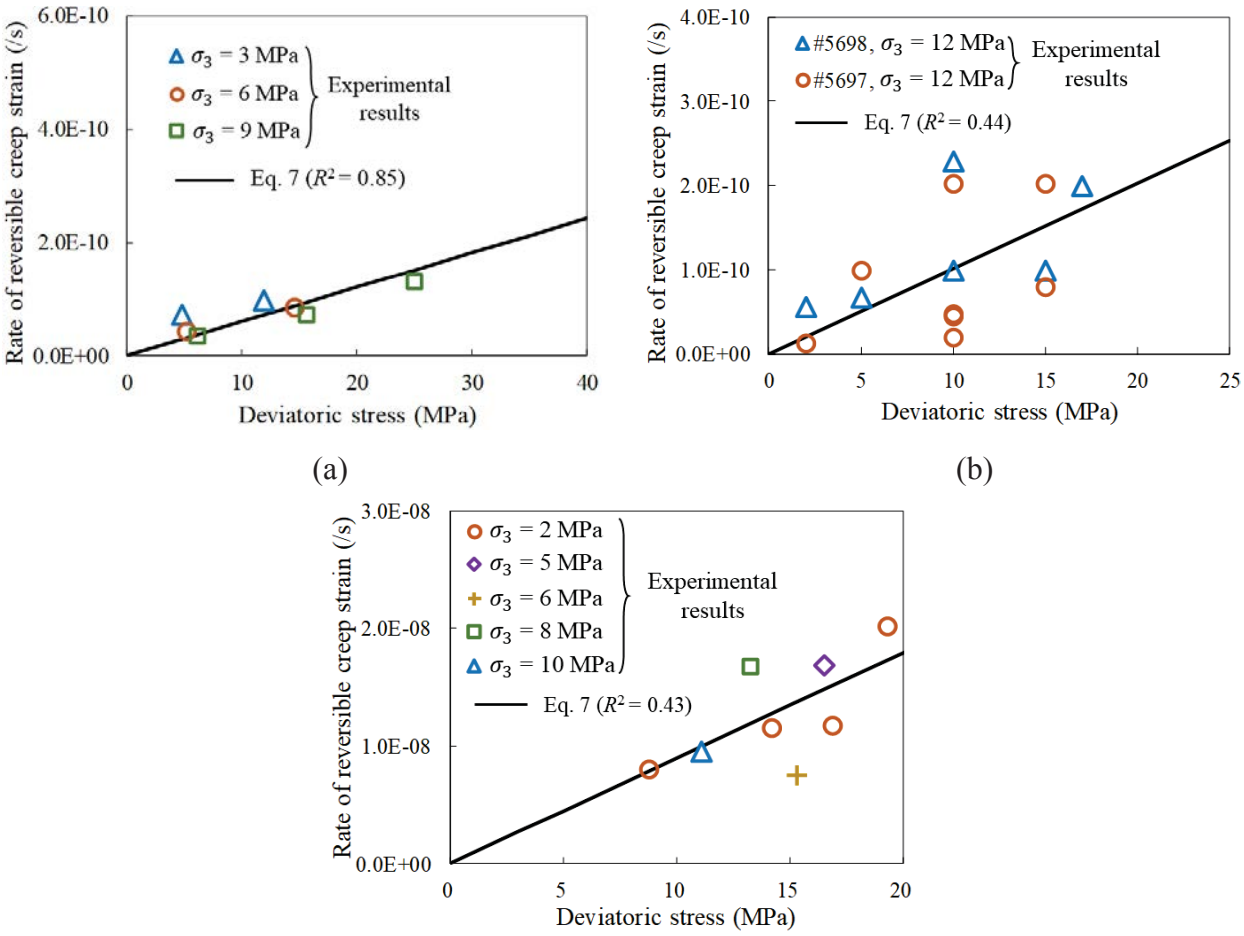

Figure 5. Variation of the measured rates of the reversible creep strain with the deviatoric stress ($\sigma_1 - \sigma_3$): (a) on a lherzolite rock under different confining stresses with model description (for experimental data under σ_3 = 6 MPa) and prediction (for experimental data under σ_3 = 3 and 9 MPa) by using Eq. 7 and $\eta_{sc} = 5.51\times10^{16}$ Pa·s (data taken from Zhao et al.[19]); (b) on Bure clayey rock under a confining stresses σ_3 = 12 MPa with model description (for #5697) and prediction (#5698) by using Eq. 7 and $\eta_{sc} = 3.30\times10^{16}$ Pa·s (data taken from Gasc-Barbier et al.[69]); (c) on a rock salt under different confining stresses with model description (for experimental data under σ_3 = 2 MPa) and prediction (for experimental data under σ_3 = 5, 6, 8 and 10 MPa) by using Eq. 7 and $\eta_{sc} = 3.71\times10^{14}$ Pa·s (data taken from Wang et al.[70]) .

To test the model (Eq. 7), experimental data of creep tests under stresses lower than the CIT of the rock are necessary to obtain the model parameter (η_{sc}) in relation with reversible creep strain.

Figure 5 shows the variation of the measured rates of reversible creep strain as a function of the deviatoric stress ($\sigma_1 - \sigma_3$) under different confining stresses when the applied stress on a

lherzolite (Fig. 5a), a Bure clayey rock (Fig. 5b), and a rock salt (Fig. 5c) is below the CIT. Description and prediction with the proposed model (Eq. 7) are also plotted on the figure. Again, CIT is considered as the start point of irreversible creep strain[43, 61] and the measured creep strain below the CIT is taken as reversible creep strain. It should be noted that the experimental data shown in the figure were taken from published papers[19, 69, 70], in which no distinction was made between the reversible and irreversible creep strains. In addition, no measurements or observations were reported in the papers to allow the determination of CIT. Thus, a value of CIT equaling to 50% of the short-term strength[13, 62] was initially taken for all of the three cases. However, a nonlinearity and confining stress dependency were observed in the case of lherzolite, indicating a largely overestimate of the CIT value. A value of CIT equaling to 30% of the short-term strength is finally taken for the case of lherzolite (Fig. 5a). Relatively good agreements are obtained between the experimental results and the proposed model (Eq. 7) in the three cases. The relationship between the rates of reversible creep strain and the deviatoric stress can be considered as more or less linear, despite the important dispersion of the experimental data observed in Figures 5b and 5c; these are probably due to imprecise measurements of the too small rates of reversible creep strains.

2.3.2 Rate of irreversible creep strain

As mentioned in Section 2.3, subcritical crack growth takes place and irreversible creep strain occurs once the applied stress exceeds the CIT. The rates of irreversible creep strain can be obtained by subtracting the rate of reversible creep strain from the rate of total creep strain. The rates of irreversible creep strain are considered to be proportional to the subcritical crack growth velocity V, which is usually related to the stress intensity factor K_i as follows[62, 71]:

$$V = A_1\left(\frac{\langle K_i - K_0\rangle}{K_c - K_0}\right)^{n_1} \tag{8}$$

where A_1 and n_1 are two material parameters; K_0 is the threshold of stress intensity factor for crack extension; K_c is the critical value of K_i, corresponding to the maximum velocity of crack growth; $\langle X\rangle = (X + |X|)/2$ is the Macaulay brackets.

Eq. 8 is difficult to be directly applied because it requires the knowledge of initial crack length to calculate the stress intensity factor. To overcome this difficulty, the following expression can be used to obtain the subcritical crack growth velocity V by considering the similarity between the microscopic and macroscopic conditions[62, 64]:

$$V = A_2\left(\frac{\langle\sigma_a - \sigma_{CI}\rangle}{\sigma_c - \sigma_{CI}}\right)^n \tag{9}$$

where A_2 and n are material parameters; σ_a is the applied deviatoric stress (σ_1-σ_3); σ_{CI} is the value of CIT in terms of deviatoric stress; σ_c denotes the short-term strength in terms of deviatoric stress as follows[72]:

$$\sigma_c = \sigma_{STF} - \sigma_3 \tag{10}$$

where σ_{STF} is the short-term strength under confining pressure σ_3, expressed as follows according to the Mohr-Coulomb criterion:

$$\sigma_{STF} = \frac{1+\sin\phi}{1-\sin\phi}\cdot\sigma_3 + 2c\cdot\frac{\cos\phi}{1-\sin\phi} \tag{11}$$

Since the rate of irreversible creep strain $\dot{\varepsilon}_{sc}^{ir}$ is proportional to the subcritical crack growth velocity V (Eq. 9), it can be written as:

$$\dot{\varepsilon}_{sc}^{ir} = A_{sc}\left(\frac{\langle\sigma_1 - \sigma_3 - \sigma_{CI}\rangle}{\sigma_{STF} - \sigma_3 - \sigma_{CI}}\right)^n \tag{12}$$

where A_{sc} (s^{-1}) is a material parameter.

Introducing Eqs. 10 and 11 into Eq. 12 leads to the rate of the irreversible creep strain as follows:

$$\dot{\varepsilon}_{sc}^{ir} = A_{sc}\left[f^*(\sigma_1, \sigma_3, c, \phi)\right]^n \tag{13}$$

where $f^*(\sigma_1, \sigma_3, c, \phi)$ (noted as f^* for simplification) is a function of normalized stress expressed as follows:

$$f^* = \frac{\langle\sigma_a - \sigma_{CI}\rangle}{\sigma_c - \sigma_{CI}} \tag{14}$$

or

$$f^* = \frac{\langle(1-\sin\phi)\cdot(\sigma_1-\sigma_3) - 2m\cdot(\sigma_3\cdot\sin\phi + c\cdot\cos\phi)\rangle}{2(1-m)(\sigma_3\cdot\sin\phi + c\cdot\cos\phi)} \tag{15}$$

after considering $\sigma_{CI} = m \cdot \sigma_c$ ($0.3 \leq m \leq 0.7$).

Function f^* is defined to describe the rate of irreversible creep strain during the secondary creep stage. Its value ranges from 0 to 1 ($0 \leq f^* < 1$). When its value equals to 0, the applied deviatoric stress is lower than or equal to the CIT and the rate of irreversible creep strain is zero. When its value is higher than zero and lower than one, the rate of irreversible creep strain increases as the value of f^* increases. When the value of f^* is equal to one (i.e. $\sigma_a = \sigma_c$), failure occurs instantaneously without any delay. The rock does not exhibit secondary creep stage. Thus, the value of f^* should be smaller than but not equal to one.

To test the capacity of the model (Eq. 13), the experimental data should contain measured cohesion and friction angle. Alternatively, the ratio between the applied stress and short-term (peak) strength should be available to obtain an estimation of the value of f^*. The model parameters A_{sc} and n can then be obtained through curve-fitting on experimental results.

Figure 6 shows the variation of the rates of irreversible creep strain of different rocks as a function of f^*, using experimental results available in the literature. The description and prediction using the new model (Eq. 13) are also presented in the figure. In most of the previous studies, only the rates of total creep strain were reported. The rates of irreversible creep strain have to be obtained by subtracting the rate of reversible creep strain calculated with Eq. 7 as shown in Figure 4 from the rate of the total creep strain. For the lherzolite (Figure 6(a)) and schist (Figure 6(c)), the rates of reversible creep strain can be estimated by using the viscosity coefficients $\eta_{SC}^{(c)}$ obtained by applying the curve-fitting technique on the experimental results below the CIT point. For the other rocks (Figures 6(b), 6(d), 6(e) and 6(f)), the viscosity coefficient of similar rocks $\eta_{SC}^{(r)}$ is used because there are no experimental results below the CIT point. Parameters A_{sc} and n in Figure 6 are obtained by using curve fitting technique on the experimental results of one confining pressure. The calibrated model (Eq. 13 with the obtained model parameters) is then used to predict the experimental results under different confining pressures (except Figure 6(b), which contains only one set of experimental results). For the cases of Figures 6(b), 6(d), 6(e) and 6(f), the cohesion and friction angle are not available while the ratio σ_a/σ_c can be found in the respective references[20, 73-

[75]. The values of f^* for these figures are estimated by Eq. 14 considering $\sigma_{CI} = \sigma_c/2$ (i.e. $m = 0.5$).

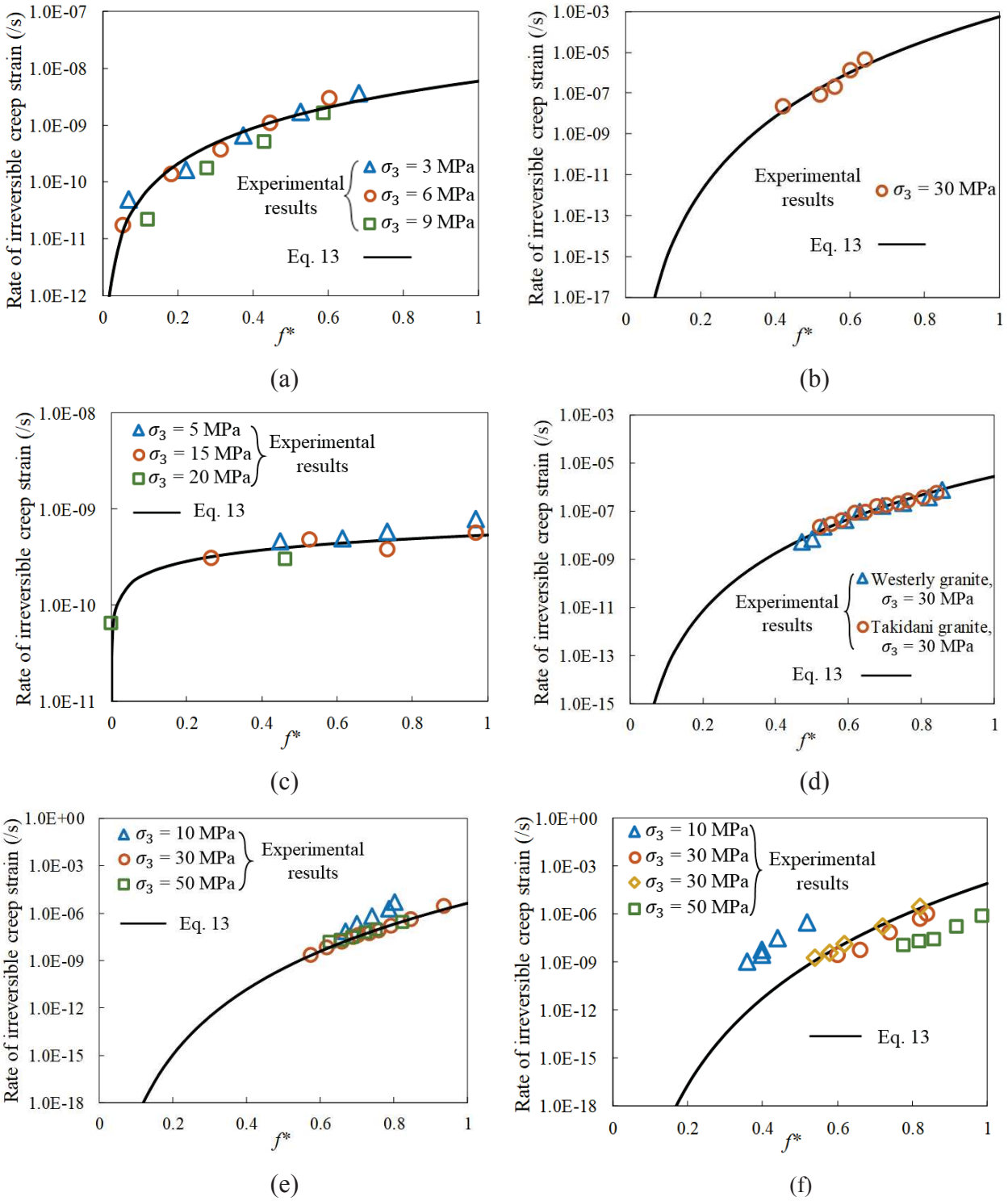

Figure 6. Variation of the rates of the irreversible creep strain with the normalized stress f^* under different confining stresses: (a) on a lherzolite with model description (for data under σ_3=6 MPa)

and prediction (for data under σ_3=3 and 9 MPa) by using Eq. 13 and c=14.2 MPa, ϕ=35.4º, A_{sc}=5.87×10^{-9} s^{-1}, n=2.07, $\eta_{SC}^{(c)}$= 5.51×10^{16} Pa·s, m=0.3 (data processed based on Zhao et al.[19]); (b) on Tavel limestone with model description by using Eq. 13 and A_{sc}=5.46×10^{-4} /s, n=12.3, $\eta_{SC}^{(r)}$=5.84×10^{16} Pa·s, m=0.5 (data processed based on Brantut et al.[20]); (c) on a schist with model description (for data under σ_3=15 MPa) and prediction (for data under σ_3=5 and 20 MPa) by using Eq. 13 and c=6.09 MPa, ϕ=34.76º, A_{sc}=5.40×10^{-10} /s, n=0.391, $\eta_{SC}^{(c)}$=7.99×10^{16} Pa·s, m=0.5 (data processed based on Liu et al.[21]); (d) on Westerly granite and Takidani granite with model description (for Westerly granite) and prediction (for Takidani granite) by using Eq. 13 and A_{sc}=2.66×10^{-6} /s, n=8.03, $\eta_{SC}^{(r)}$=5.50×10^{18} Pa·s, m=0.5 (data processed based on Brantut et al.[20, 73]); (e) on Etna basalt with model description (for data under σ_3=30 MPa) and prediction (for data under σ_3=10 and 50MPa) by using Eq. 13 and A_{sc}=4.62×10^{-6} /s, n=13.7, $\eta_{SC}^{(r)}$=5.50×10^{18} Pa·s, m=0.5 (data processed based on Heap et al.[74]); (f) on Darley Dale sandstone with model description (for data under σ_3=30 MPa) and prediction (for data under σ_3=10 and 50MPa) by using Eq. 13 and A_{sc}=8.27×10^{-5} /s, n=18.0, $\eta_{SC}^{(r)}$=1.51×10^{17} Pa·s, m=0.5 (data processed based on Heap et al.[75]). ($\eta_{SC}^{(r)}$ in (b) is from Chin and Rogers[76], in (d), (e) and (f) are from Paraskevopoulou et al.[16]. $\eta_{SC}^{(c)}$ in (a) and (c) are calculated in this study)

The results show that the calibrated model (Eq. 13 with the curve-fitting parameters) predicts well the rates of irreversible creep strain as shown in Figure 6(a) for the confining pressures of 3 and 9 MPa, Figure 6(c) for the confining pressures of 5 and 20 MPa, Figure 6(d) for Takidani granite under confining pressure of 30 MPa, Figure 6(e) for the confining pressures of 10 and 50 MPa. In these cases, the curves for a given rock merge into each other under different confining stresses. The predictive capability of the calibrated model is verified. The calibrated model can then be used to predict the rates of irreversible creep strains under different confining pressures. However, an exception is seen for Darley Dale sandstone (Figure 6(f)). The experimental results do not merge into one curve under the different confining stresses. More work is necessary to understand these results. A possible reason is the inaccuracy associated with an assumed viscosity coefficient of similar rocks taken from the literature[16].

2.3.3 Total creep strain of the secondary creep stage

Considering the reversible (Eq. 7) and irreversible (Eq. 13) creep strains leads to the total creep strains of the secondary creep strain as follows:

$$\varepsilon_{sc} = \left[\frac{\sigma_1 - \sigma_3}{3\eta_{sc}} + A_{sc}\left(\frac{\langle \sigma_1 - \sigma_3 - \sigma_{CI} \rangle}{\sigma_c - \sigma_{CI}}\right)^n\right] \cdot t \quad (16)$$

Figure 7 shows the variation of the measured rates of the total creep strain of the secondary creep stage as a function of the deviatoric stress, obtained by Zhao et al.[19]. The model parameters of Eq. 16 were first obtained by using curve fitting technique on the experimental results under the confining pressure of 3MPa. The calibrated model (Eq. 16 with the obtained model parameters) is then applied to predict the experimental results under the confining pressure of 6 MPa. The good agreements between the model and experimental results indicate that the proposed model can be used to describe and predict the creep strain rates of rocks under different stress states.

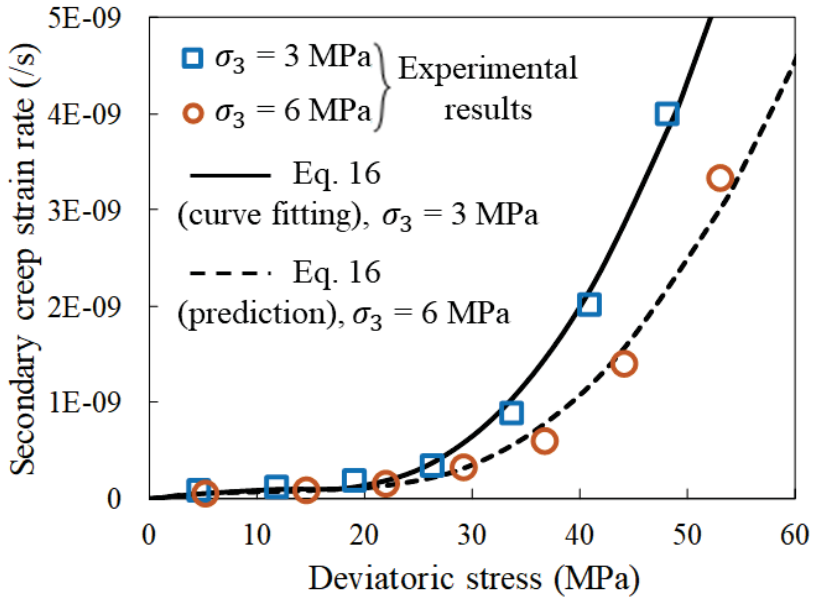

Figure 7. Variation of the measured secondary creep strain rate with the deviatoric stress ($\sigma_1 - \sigma_3$) under different confining stresses with model description (for data under σ_3=3 MPa) and prediction (for data under σ_3=6 MPa) of Eq. 16 using c=14.2 MPa, ϕ=35.4º, A_{sc}=8.91×10^{-9} /s, n=2.31, $\eta_{SC}^{(c)}$=3.12×10^{16} Pa·s, m=0.3 (data taken from Zhao et al.[19]).

2.4 Time to failure

In Figure 2, one sees that the subcritical cracks propagation is randomly and almost uniformly distributed throughout the rock as indicated by the AE activities before the tertiary (accelerating)

409 creep stage. During the tertiary creep stage, the coalescence of the AE activities appears around an
410 inclined critical plane[23, 75], which finally becomes the plane of failure as the case of a rock
411 submitted to conventional triaxial compression test conditions.[20, 21] This is a typical feature of
412 frictional geomaterials. In addition, the time to failure of the tertiary creep stage of rocks depends
413 on the applied stress.[14, 16, 77] The UC element shown in Figure 3 is proposed here to capture these
414 features, including the time to failure of rocks when the rock is submitted to a stress state higher
415 than the CIT but lower than the peak strength.

416 With the growth of subcritical cracks, the area of intact rock (contact area) decreases and the
417 internal stress on the area of intact rock increases.[78] Delayed failure occurs when the internal stress
418 state reaches a critical state defined by the Mohr-Coulomb criterion. This is the physical basis of
419 the UCC creep model for time to failure. Moreover, the following assumptions are made in the
420 model:

421 1) The interaction between micro cracks is not considered.
422 2) The area affected by cracks is independent on the initial angle of inclination.
423 3) The reduction speed of the contact area is proportional to subcritical crack growth velocity V.
424 4) At failure, the Mohr-Coulomb criterion applies.

425 Figure 8 shows a simplified two-dimensional micro element at the center of a rock sample in
426 creep process with the presence of only one micro crack. The rock around the micro crack can be
427 divided into three zones:

428 1) Subcritical crack extension zone where the crack continues to extend due to the crack wing
429 propagation, resulting in decrease of the contact area;
430 2) Affected zone. In this area, the stresses increase as the contact area in the subcritical crack
431 extension zone decreases;
432 3) Intact zone. This area is far enough from the subcritical crack extension zone. The rock in this
433 zone is in stationary (secondary) creep stage. However, it can transfer into tertiary creep stage
434 if the affected zone fails. In this case, the propagation of the subcritical crack extension and the
435 affected zones can accelerate and considerably reduce the intact zone until to the failure of the

436 whole rock.

437

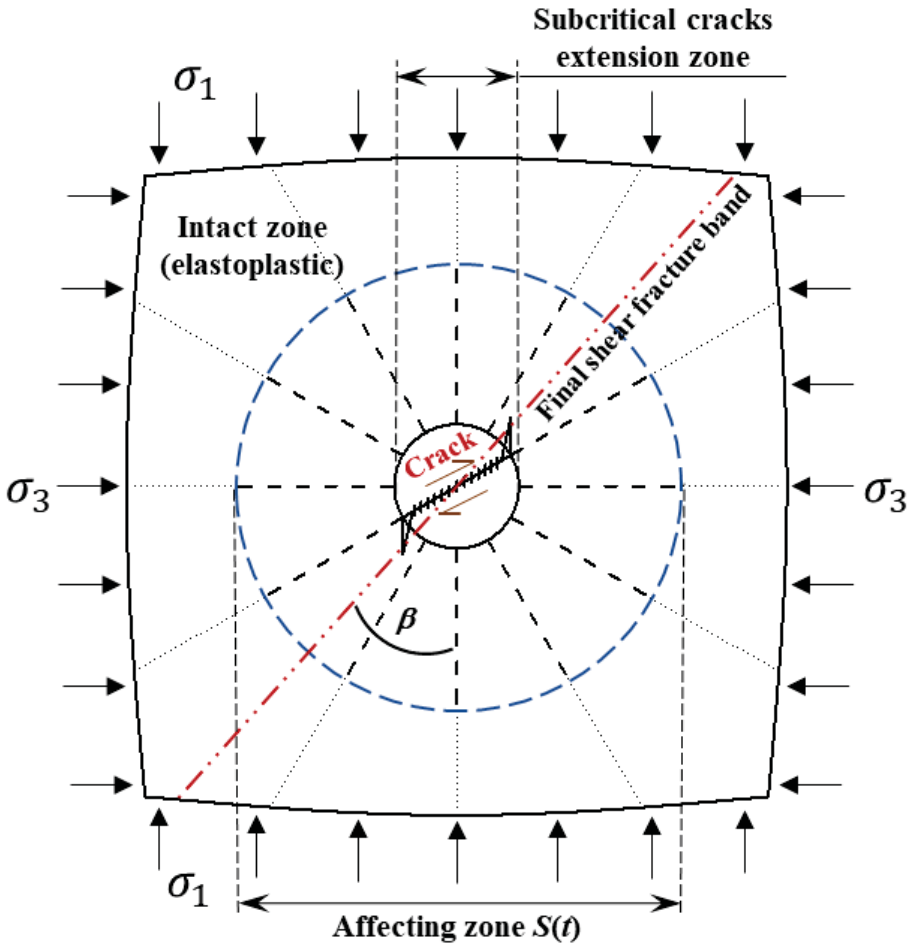

438

439 Figure 8. The simplified model based on the micro element from center of a rock sample in the
440 tertiary creep stage of creep process.

441

442 Now, one considers a micro crack making an angle of β (°) with the major principal stress σ_1.
443 Along the crack plane, the normal (σ_t^β) and shear (τ_t^β) stresses can be represented by a point on the
444 Mohr circle of the stress state (σ_3, σ_1), which makes an angle of θ (= ½β) with the normal stress
445 axis as shown in Figure 9. At a given time t, they can be expressed as follows within the affected
446 zone:

447 $$\tau_t^\beta = \frac{F_\tau^\beta}{S(t)} \quad (17)$$

448 $$\sigma_t^\beta = \frac{F_\sigma^\beta}{S(t)} \quad (18)$$

where F_τ^β (N) and F_σ^β (N) are the shear and normal forces, respectively; $S(t)$ (m^2) is the area of the affected zone.

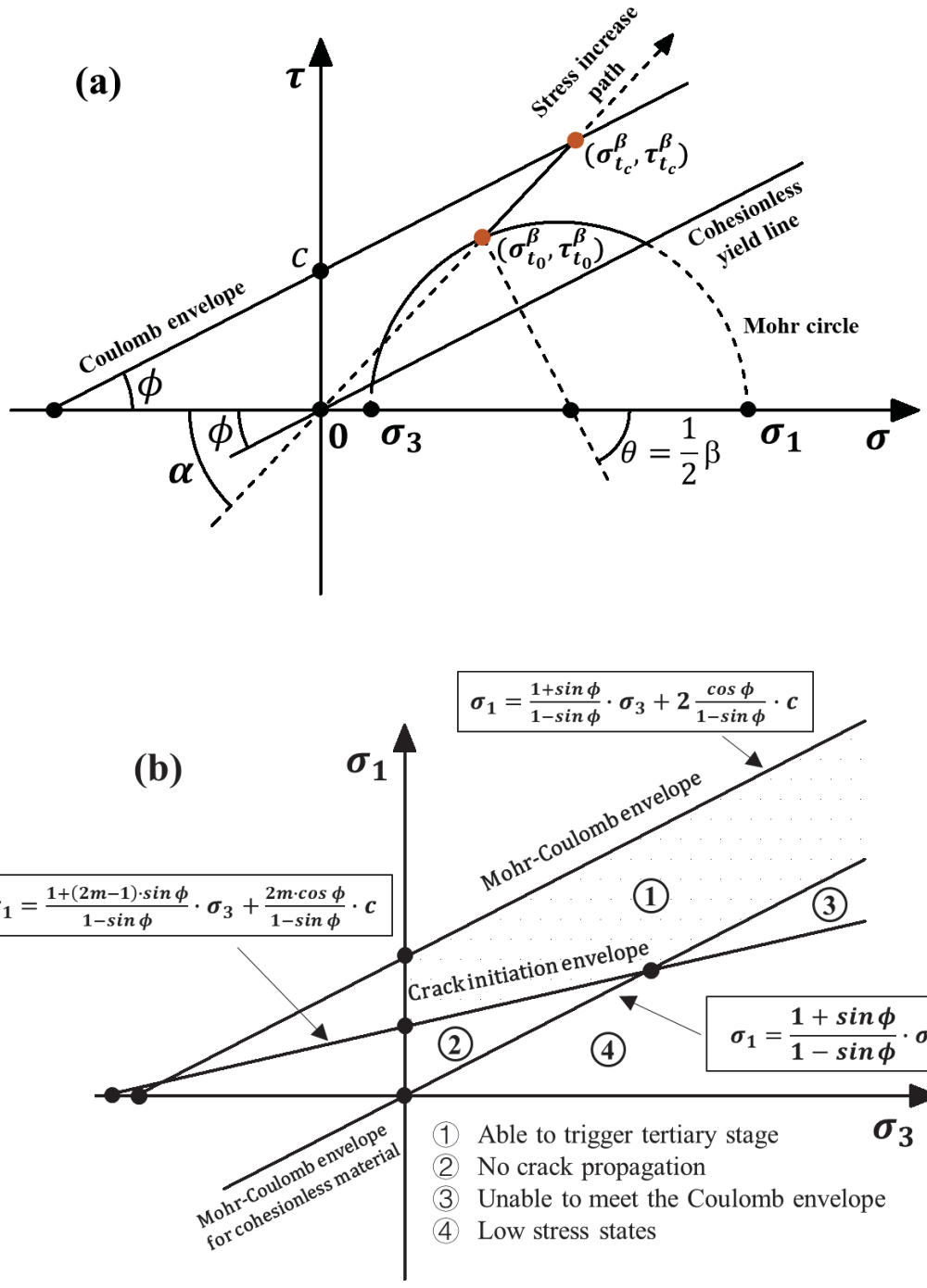

Figure 9. Illustration of (a) internal stress path associated with the crack extension in Mohr plane and (b) stress criteria for the occurrence of the tertiary creep stage.

Figure 9(a) shows the evolution of the stress state from ($\sigma_{t_0}^{\beta}$, $\tau_{t_0}^{\beta}$) to (σ_{t}^{β}, τ_{t}^{β}) when time passes from t_0 to t, following a line making an angle of α with the normal stress σ axis:

$$\tan\alpha = \frac{d\tau_t^{\beta}}{d\sigma_t^{\beta}} = \frac{F_{\tau}^{\beta}}{F_{\sigma}^{\beta}} = \frac{\tau_{t_0}^{\beta}}{\sigma_{t_0}^{\beta}} \tag{19}$$

The initial normal and shear stresses can be expressed as:

$$\tau_{t_0}^{\beta} = \frac{1}{2}\cdot(\sigma_1 - \sigma_3)\cdot\sin\theta; \tag{20}$$

$$\sigma_{t_0}^{\beta} = \frac{1}{2}\cdot[\sigma_1 + \sigma_3 - (\sigma_1 - \sigma_3)\cdot\cos\theta] \tag{21}$$

One sees that the stress path line can meet the Coulomb criterion envelope only when the applied stress is higher than the CIT and the value of angle α is larger than the friction angle ϕ.

Figure 9(b) shows the different zones surrounded by the Mohr-Coulomb envelop ($\sigma_1 = \frac{1+\sin\phi}{1-\sin\phi}\cdot\sigma_3 + 2\frac{\cos\phi}{1-\sin\phi}\cdot c$), the CIT line ($\sigma_1 = \frac{1+(2m-1)\cdot sin\,\phi}{1-sin\,\phi}\cdot\sigma_3 + \frac{2m\cdot cos\,\phi}{1-sin\,\phi}\cdot c$) and the cohesionless yield line ($\sigma_1 = \frac{1+\sin\phi}{1-\sin\phi}\cdot\sigma_3$). When the cohesion is very low, Zone 1 (susceptible to the tertiary creep) will be very thin and close to the peak strength line. This means that the stresses applied on low cohesion rocks must be carefully controlled to achieve a tertiary creep stage. This explains why low cohesion rocks such as rock salts usually exhibit ductile behavior and much less brittle behavior and shear failure[7].

Considering the case when the internal stresses increase along the stress path and meet the Coulomb envelop leads to the following expressions:

$$\begin{cases} \tau_{t_c}^{\beta} = \sigma_{t_c}^{\beta}\cdot tan\,\alpha \\ \tau_{t_c}^{\beta} = \sigma_{t_c}^{\beta}\cdot tan\,\phi + c \end{cases} \tag{22}$$

where $\tau_{t_c}^{\beta}$ and $\sigma_{t_c}^{\beta}$ are the critical shear and normal stresses, respectively.

From Eq. 22, one can express the critical shear stress $\tau_{t_c}^{\beta}$ as follows:

$$\tau_{t_c}^{\beta} = \frac{tan\,\alpha}{tan\,\alpha - \tan\phi}\cdot c \tag{23}$$

Introducing Eqs. 19 ($\tan\alpha = \frac{\tau_{t_0}^{\beta}}{\sigma_{t_0}^{\beta}}$) 20, and 21 into Eq. 23 leads to:

$$\tau_{t_c}^{\beta} = \frac{(\sigma_1 - \sigma_3)\cdot\sin\theta}{(\sigma_1 - \sigma_3)\cdot\sin\theta - [\sigma_1 + \sigma_3 - (\sigma_1 - \sigma_3)\cdot\cos\theta]\cdot\tan\phi}\cdot c \tag{24}$$

The time to failure t_f can be written as:

$$t_f = \frac{\tau_{t_c}^{\beta} - \tau_{t_0}^{\beta}}{V_{\tau}^{\beta}} \tag{25}$$

where $\tau_{t_0}^{\beta}$ is the initial shear stress at time t_0; $\tau_{t_c}^{\beta}$ is the critical shear stress at time t_c; V_{τ}^{β} is the increase rate of shear stress, expressed as follows:

$$V_{\tau}^{\beta} = \frac{\partial\tau_t^{\beta}}{\partial t} = -\frac{F_{\tau}^{\beta}}{S(t)}\cdot\frac{1}{S(t)}\cdot\dot{S(t)} \tag{26}$$

where $\dot{S(t)}$ denotes the decrease rate of the contact area $S(t)$.

Considering Eq. 9, $\dot{S(t)}$ can be given as the following expression:

$$\dot{S(t)} = A_{tc}\left(\frac{\langle(1-\sin\phi)\cdot(\sigma_1-\sigma_3) - 2m\cdot(\sigma_3\cdot\sin\phi + c\cdot\cos\phi)\rangle}{2(1-m)(\sigma_3\cdot\sin\phi + c\cdot\cos\phi)}\right)^n \tag{27}$$

where A_{tc} (s^{-1}) is a material parameter.

To avoid the shear stress growth rate becoming an overly complicated function of θ and t, the reduction in the contact area of the affected zone (Figure 8) associated with the crack growth is considered as very small and the value of $S(t)$ in Eq. 26 is roughly considered to be equal to $S(t_0)$. Eq. 26 can then be simplified as follows:

$$V_{\tau}^{\beta} = \frac{\partial\tau_t^{\beta}}{\partial t} = -\tau_{t0}^{\beta}\cdot\frac{1}{S(t_0)}\cdot\dot{S(t)} \tag{28}$$

To make the analytical solution possible, one assumes the area of the micro crack to be unity at the beginning of the irreversible creep process t_0 (i.e. $S(t_0) = 1$). Introducing Eqs. 20, 24, 27 and 28 into Eq. 25, one obtains the time to failure as:

$$t_f = \frac{\frac{2}{\Gamma(\theta)}\cdot c - 1}{A_{tc}\left(\frac{\langle(1-\sin\phi)\cdot(\sigma_1-\sigma_3) - 2m\cdot(\sigma_3\cdot\sin\phi + c\cdot\cos\phi)\rangle}{2(1-m)(\sigma_3\cdot\sin\phi + c\cdot\cos\phi)}\right)^n} \tag{29}$$

where function $\Gamma(\theta)$ is expressed as follows:

$$\Gamma(\theta) = (\sigma_1 - \sigma_3)\cdot\sin\theta - [\sigma_1 + \sigma_3 - (\sigma_1 - \sigma_3)\cdot\cos\theta]\cdot\tan\phi \tag{30}$$

The minimum time to failure can then be obtained by imposing $\frac{dt_f}{d\theta} = 0$. This leads to:

$$\frac{d\Gamma(\theta)}{d\theta} = (\sigma_1 - \sigma_3) \cdot \cos\theta_c - (\sigma_1 - \sigma_3) \cdot \sin\theta_c \cdot \tan\phi = 0 \tag{31}$$

where θ_c is the critical angle of the stress state in Mohr plane, corresponding to the critical plane β_c in the rock sample. The latter can then be identified as:

$$\beta_c = \frac{\theta_c}{2} = 45° - \frac{\phi}{2} \tag{32}$$

This angle is the same as that in conventional triaxial compression tests. This explains well why the failure plane during the tertiary creep stage is very similar to that of conventional triaxial compression tests. But the meaning is that among the numerous micro cracks, the one making an angle of 45°-ϕ/2 with the major principal stress σ_1 will be the first becoming instable.

The tertiary creep strain of UCC model can then be written as:

$$\varepsilon_{tc} = C(\sigma_1,\sigma_3,\phi) \cdot \left\langle t - \frac{\tau_{t_c}^{\beta_c} - \tau_{t_0}^{\beta_c}}{V_\tau^{\beta_c}} \right\rangle^0 \cdot F(t) \tag{33}$$

where $C(\sigma_1, \sigma_3, \phi)$ is an additional criterion for tertiary creep (see the Cohesionless yield line in Figure 9), given as:

$$C(\sigma_1,\sigma_3,\phi) = \left\langle \sigma_1 - \frac{1+\sin\phi}{1-\sin\phi} \cdot \sigma_3 \right\rangle^0 \tag{34}$$

If the Mohr circle is below the Cohesionless yield line, it will be impossible for the stress state points to touch the Coulomb envelope even though the stresses can increase with the reduction of the contact area.

Function F(t) is introduced to control the shape of time−creep strain curve in the tertiary (accelerating) creep stage. It can be given as:

$$F(t) = \gamma \cdot \left(\frac{t}{t_c}\right)^\lambda \tag{35}$$

where γ and λ are two parameters.

To test the model (Eq. 29), experimental data required to test Eq. 13 are necessary. Moreover, the experimental data should contain creep strain results under different confining stresses to predict the time to failure.

Figure 10 shows the time to failure of Barre granite as a function of f^* under different stress states, obtained in laboratory tests by Kranz.[72] The model parameters of the UCC creep model are first obtained by applying curve-fitting technique on the experimental results under a confining pressure of 0.1 MPa (solid line). The UCC creep model along with the obtained model parameters are then used to predict the time to failure under a confining pressure of 101 MPa (dash line). It can be seen that the agreements between the experimental results and the model description and prediction are quite good. The UCC creep model can thus be used to describe and predict the time to failure of rocks under different deviatoric and confining stresses.

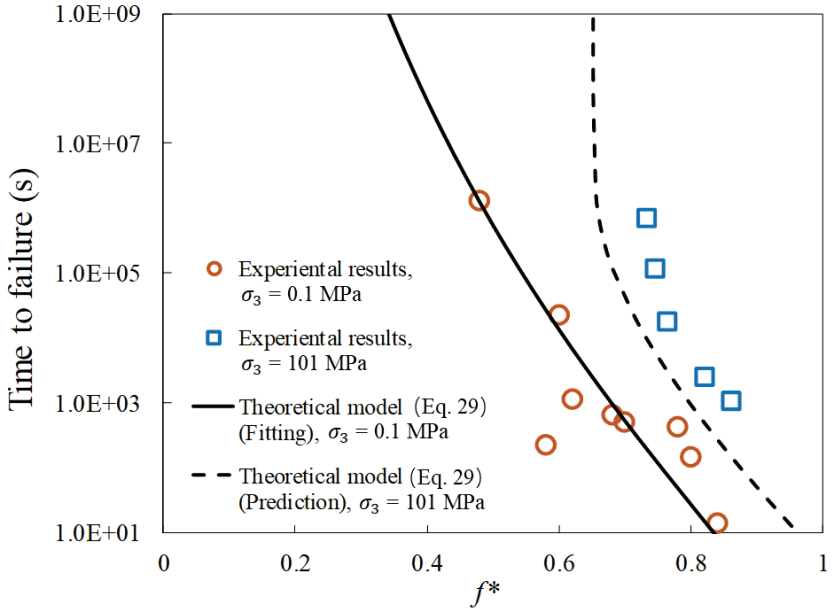

Figure 10. Variation of the measured time to failure with f^* under different confining stresses with UCC creep model description (for data under σ_3 = 0.1 MPa) and prediction (for data under σ_3 = 101 MPa) by using Eq. 29 and c = 44.3 MPa, ϕ = 46.1°, A_{tc}=0.25 s^{-1}, n=18.71, m=0.5 (experimental results taken from Kranz[72]).

2.5 Total axial strain

Introducing Eqs. 4, 5, 16 and 33 into Eq. 1, the total axial strain of the UCC creep model can be given as:

$$\varepsilon_t = \frac{\sigma_1-\sigma_3}{9K_e} + \frac{\sigma_1-\sigma_3}{3G_e} + \frac{\sigma_1-\sigma_3}{3G_K}\left[1-exp\left(-\frac{G_K\cdot t}{\eta_K}\right)\right] + \left[\frac{(\sigma_1-\sigma_3)}{3\eta_{sc}} + A_{sc}\left(\frac{\langle\sigma_1-\sigma_3-\sigma_{CI}\rangle}{\sigma_c-\sigma_{CI}}\right)^n\right]\cdot t + C$$

$$(\sigma_1,\sigma_3,\phi)\cdot\left\langle t-\frac{\tau_{t_c}^{\beta_c}-\tau_{t_0}^{\beta_c}}{V_\tau^{\beta_c}}\right\rangle^0\cdot F(t) \tag{36}$$

3. Application of the UCC creep model

3.1 Parameter identification

To use UCC creep model (Eq. 36), parameters K_e, G_e, G_K, η_K, η_{sc}, A_{sc}, A_{tc}, n, γ, and λ need to be identified.

K_e and G_e can be obtained from elastic modulus E and Poisson's ratio υ as follows:

$$G_e=\frac{E}{2(1+\upsilon)} \tag{37}$$

$$K_e=\frac{E}{3(1-2\upsilon)} \tag{38}$$

In absence of E and υ, their value can also be obtained by curve-fitting technique on instantaneous strain as a function of stress.

Parameters G_K and η_K can be obtained by fitting the UCC creep model with measured total creep strains as a function of time under one or several stress states.

Parameter η_{sc} can be obtained by curve-fitting on the measured rates of reversible creep strain. The creep strain under a stress state lower than the CIT is reversible creep strain. The measured CIT should be used as long as it is available. In absence of its measurement, its value can typically be taken as 50% of the short-term strength.[13, 62] However, the ratio between the CIT and short-term strength can range from 30 to 70%, as shown in Table 1.

Parameters A_{sc} and n are obtained by fitting the model with measured rates of irreversible creep strain. The rates of irreversible creep strain are obtained by subtracting the rate of reversible creep strain from the rate of total creep strain.

Parameter A_{tc} can be obtained by fitting the model with measured time to failure under one or several confining pressure levels. Parameters γ and λ are obtained by fitting the model with the measured total creep strain as a function of time.

569 **3.2 Sample application**

570 Zhao et al.[19] conducted a series of creep tests on lherzolite cylinder rock samples having a
571 diameter of 50 mm and a height of 100 mm. Axial loads were exercised through a servo-controlled
572 rheological test machine. The axial strains were measured by a linear variable displacement
573 transducer (LVDT). Cyclic increment loading and unloading creep tests were conducted. The axial
574 pressure was loaded at a rate of 0.03 MPa/s until the targeted stress level, which was maintained
575 constant for a duration of 90 h. After that, unloading was processed until a zero deviatoric stress.
576 A repos period of 20 to 30 h was applied before applying a new load.

577 According to Zhao et al.[19], fifteen triaxial compression tests were performed under the
578 confining pressures of 0, 3, 6, 9 and 12 MPa, respectively. However, they only presented the
579 experimental results under the confining pressure of 6 MPa at different deviatoric stress levels as
580 shown in Figure 11. These results will be used to test the description and prediction ability of the
581 proposed UCC creep model.

582 Table 2 shows the required model parameters, obtained by applying the curve-fitting
583 technique on the experimental results under the deviatoric stresses of 14.8 MPa (below the CIT,
584 20.8 MPa), 36.9 MPa and 44.2 MPa (above the CIT). It is interesting to note that the obtained bulk
585 and shear modulus are quite close to those presented by Zhao et al.[19]. These parameters are then
586 used in the UCC creep model to predict the creep behavior of the rock under other deviatoric
587 stresses.

588 The description and prediction of the UCC creep model using the model parameters shown in
589 Table 2 are plotted on Figure 12. It can be seen that the model description of the experimental
590 results under deviatoric stress of 14.8, 36.9 and 44.2 MPa are very good while the prediction of the
591 calibrated model on the experimental results under other deviatoric stresses are also quite good. It
592 should be noted that the prediction of the calibrated model (i.e. Eq. 36 with the obtained model
593 parameters shown in Table 2) on the tertiary creep stage is also good.

594

595 Table 2. Material parameters obtained by applying the curve-fitting technique on the
596 experimental results of the 2th, 5th and 6th stress levels with the confining pressure of 6 MPa,

reported by Zhao et al.[19].

c (MPa)	ϕ (°)	K_e (GPa)	G_K (GPa)	G_e (GPa)	η_K (GPa·h)	η_{sc} (GPa·h)
14.2	35.4°	6.90	6.87	4.06	19.73	9.96×10^{3}
A_{sc} (h^{-1})	A_{tc} (h^{-1})	n	γ	λ	m	
7.76×10^{-6}	0.024	2.78	1.1×10^{-4}	195	0.3	

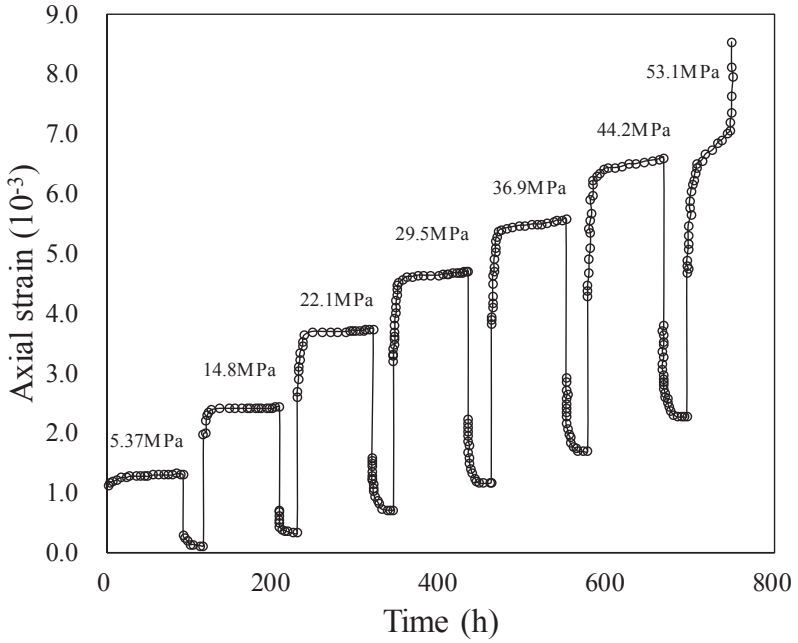

Figure 11. Original axial strain data under the confining pressure of 6 MPa and different deviatoric stresses (data taken from Zhao et al.[19]).

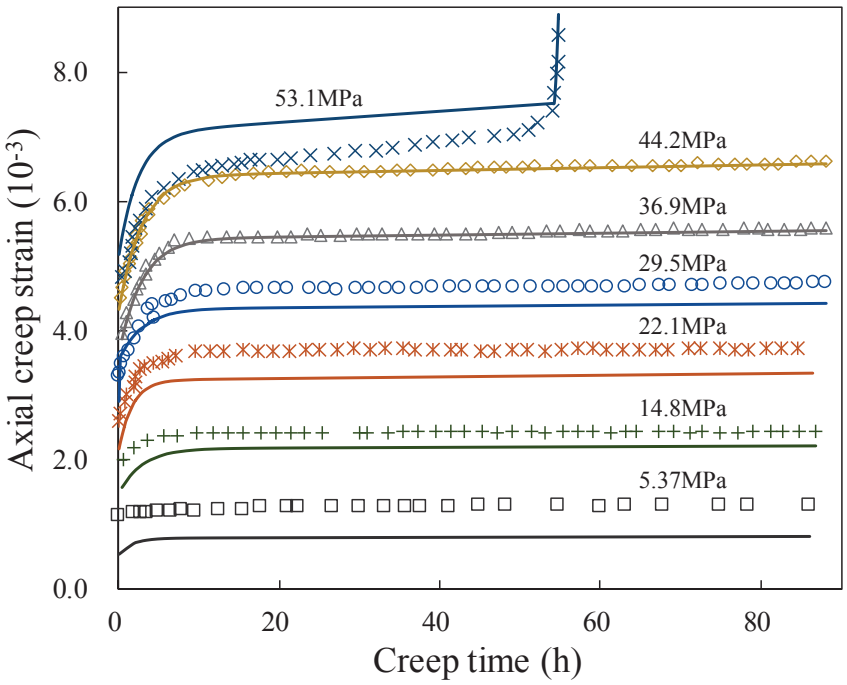

Figure 12. Experimental results (points) of the strain evolutions of a cylinder rock under different axial stresses at the confining pressure of 6 MPa (data taken from Zhao et al.[19]); the solid lines correspond to the three descriptions and four predictions of the UCC creep model using the model parameters given in Table 2.

4. Discussion

In this study, a new creep model, called UCC creep model is proposed to describe and predict the creep strain, rate of creep strain and time to failure of rocks. The results show that the UCC creep model is capable to describe and predict the creep strain and time to failure of rocks under different stress states. However, some hypotheses involved in the model need to be discussed:

1) The application of the model requires the knowledge of CIT. For a given rock, the CIT value can be determined as the start of deviation of the axial stress-radial strain curves from the linearity, start of acoustic emission, or start of dilation. The measured value should be used in the model as long as it is available. In absence of its measurement, it can be simply taken as 50% of the short-term strength for most cases[13, 62]. However, the ratio between the CIT and short-term strength can range from 30 to 70%, as shown in Table 1.
2) The change in the internal stresses was only attributed to the reduction of the contact area, which was in turn associated with the extension of micro cracks (irreversible creep strain). In

the future, more work is necessary to take into account the interaction between micro cracks.[78, 79]

3) The distribution of initial cracks and the space orientations of micro cracks were not considered in this study. They should be further studied in future.[49]
4) In this study, the relationship between the applied stress and the micro crack extension velocity was described by Eq. 8. This is an equation based on the crack extension in the glass which is homogeneous and isotropic. However, most rocks are of non-homogeneous and anisotropic properties. Therefore, this relationship will need to be further investigated in future study.
5) AE in rock samples during creep tests was generally observed in the primary and secondary creep stages. In this study, the irreversible creep strain was only considered in the secondary creep stage because the secondary creep stage is dominant in the long-term deformation. Nevertheless, the irreversible creep strain in the primary creep stage needs to be considered in the future.
6) In this study, the affected zone of cracks was considered as independent on the initial inclination angle of micro cracks. More work is needed to investigate its validity and impact on the proposed model.
7) In Eq. 28, a simplification has been made by assuming a negligible effect of the crack extension on $S(t)$. $S(t)$ was loosely considered to be equal to $S(t_0)$, which was assumed to be unity area. This simplifying assumption is necessary to avoid overly complicated derivations. Other forms of $S(t)$ are expected to be studied in future to improve the model.

In this study, the tests of the capacity of the model were made by using limited data available in the literature. More experimental works are needed on a wider range of rocks. Moreover, the UCC creep model was developed by considering conventional triaxial compression test conditions. It is known that the intermediate principal stress can affect the mechanical behavior of rocks. An improvement of the UCC creep model is expected by taking the intermediate principal stress into consideration. Its validation requires in turn more creep tests under true triaxial compression test conditions.

649 Finally, in order for the proposed model to be useful in practice, its implementation in a
650 numerical code is necessary.[80, 81]
651
652 ## 5. Conclusions
653 In this paper, a new model called UCC creep model is proposed to represent and predict creep
654 strain and time to failure of rocks under different stress states. It makes distinction between the
655 reversible and irreversible creep strains in the secondary creep stage. The former was associated
656 with the visco-elasticity of rocks while the latter was related to the subcritical micro cracks growth.
657 The effects of friction angle and confining pressure on the rate of irreversible creep strain and the
658 time to failure have be considered in the model. The similarity between the failure plane of creep
659 tests and that observed in conventional triaxial compression tests is mathematically shown. With
660 the UCC creep model, the failure along the plane making an angle of $45°-\phi/2$ with the major
661 principal stress σ_1 in creep tests is explained by the fact that among the numerous micro cracks,
662 the cracks along this orientation are the first becoming instable. To test the description and
663 prediction capability of the UCC creep model against experimental results available in the literature,
664 the model parameters were first obtained by applying the curve-fitting technique on a part of the
665 available experimental results. The obtained model parameters were then used in the model (i.e.
666 calibrated model) to predict another part of the available experimental results, which were not used
667 in the curve-fitting process. The results showed that proposed UCC creep model is able to describe
668 and predict the creep strain and time to failure in creep process of rocks under different stress
669 conditions.
670
671 ## Conflict of interest
672 The authors wish to confirm that there are no known conflicts of interest associated with this
673 publication and there has been no significant financial support for this work that could have
674 influenced its outcome.
675
676 ## Acknowledgements

677 The authors acknowledge the financial support from the Natural Sciences and Engineering
678 Research Council of Canada (NSERC 402318, RGPIN-2018-06902), Fonds de recherche du
679 Québec—Nature et Technologies (FRQNT 2015-MI-191676), and industrial partners of the
680 Research Institute on Mines and the Environment (RIME UQAT-Polytechnique; http://rime-
681 irme.ca/). The first author gratefully acknowledges the financial support from China Scholar
682 Council (grant number 201706420059). The authors thank the anonymous reviewers for their
683 criticism and constructive comments that are very useful to improve the quality of the paper.
684

685 ## References

686 1. Hardy Jr H, Kim R, Stefanko R, Wang Y. Creep and microseismic activity in geologic
687 materials. In: *Proceedings of the 11th US Symposium on Rock Mechanics (USRMS)*. American
688 Rock Mechanics Association; 1969: 377-414.
689 2. Cristescu N, Hunsche U. *Time effects in rock mechanics*. Wiley New York; 1998.
690 3. Malan K. Time-dependent behaviour of hard rock in deep level gold mines. *J S Afr I Min*
691 *Metall*. 1997; 97(3): 135-147.
692 4. Malan D. Time-dependent behaviour of deep level tabular excavations in hard rock. *Rock*
693 *Mech Rock Eng*. 1999; 32(2): 123-155.
694 5. Verstrynge E, Schueremans L, Van Gemert D. Time-dependent mechanical behavior of lime-
695 mortar masonry. *Mater Struct*. 2011; 44(1): 29-42.
696 6. Ma L, Liu X, Fang Q, Xu H, Xia H, Li E, Yang S, Li, W. A new elasto-viscoplastic damage
697 model combined with the generalized Hoek–Brown failure criterion for bedded rock salt and
698 its application. *Rock Mech Rock Eng*. 2012; 46(1): 53-66.
699 7. Paraskevopoulou C, Diederichs M. Analysis of time-dependent deformation in tunnels using
700 the Convergence-Confinement Method. *Tunn Undergr Sp Tech.* 2018; 71: 62-80.
701 8. Xu T, Xu Q, Deng M, Ma T, Yang T, Tang C. A numerical analysis of rock creep-induced
702 slide: a case study from Jiweishan Mountain, China. *Environ Earth Sci*. 2014; 72(6): 2111-
703 2128.
704 9. Goodman R. *Introduction to rock mechanics*. Wiley New York; 1989.
705 10. Amitrano D, Helmstetter A. Brittle creep, damage, and time to failure in rocks. *J Geophys Res*.
706 2006; 111(B11201): 1-17.
707 11. Farmer IW. *Engineering behaviour of rocks*. Springer Science & Business Media; 2012.
708 12. Ngwenya BT, Main IG, Elphick SC, Crawford BR, Smart BGD. A constitutive law for low-
709 temperature creep of water-saturated sandstones. *J Geophys Res*. 2001; 106(B10): 21811-

710 21826.

711 13. Lajtai E, Schmidtke R. Delayed failure in rock loaded in uniaxial compression. *Rock Mech*
712 *Rock Eng*. 1986; 19(1): 11-25.

713 14. Campanella R, Vaid Y. Triaxial and plane strain creep rupture of an undisturbed clay. *Can*
714 *Geotech J*. 1974; 11(1): 1-10.

715 15. Hao S, Liu C, Wang Y, Chang F. Scaling law of average failure rate and steady-state rate in
716 rocks. *Pure Appl Geophys*. 2017; 174(6): 2199-2215.

717 16. Paraskevopoulou C, Perras M, Diederichs M, Loew S, Lam T, Jensen M. Time-dependent
718 behaviour of brittle rocks based on static load laboratory tests. *Geotech Geologic Eng*. 2017;
719 36(1): 337-376.

720 17. Li Y, Xia C. Time-dependent tests on intact rocks in uniaxial compression. *Int J Rock Mech*
721 *Min Sci*. 2000; 37(3): 467-475.

722 18. Sterpi D, Gioda G. Visco-plastic behaviour around advancing tunnels in squeezing rock. *Rock*
723 *Mech Rock Eng*. 2009; 42(2): 319-339.

724 19. Zhao Y, Wang Y, Wang W, Wan W, Tang J. Modeling of non-linear rheological behavior of
725 hard rock using triaxial rheological experiment. *Int J Rock Mech Min Sci*. 2017; 93: 66-75.

726 20. Brantut N, Heap M, Meredith P, Baud P. Time-dependent cracking and brittle creep in crustal
727 rocks: A review. *J Struct Geol*. 2013; 52: 17-43.

728 21. Liu H, Xie H, He J, Xiao M, Zhuo L. Nonlinear creep damage constitutive model for soft
729 rocks. *Mech Time-Depend Mater*. 2016; 21(1): 73-96.

730 22. Hirata T, Satoh T, Ito K. Fractal structure of spatial distribution of microfracturing in rock.
731 *Geophys J Int*. 1987; 90(2): 369-374.

732 23. Lei X, Kusunose K, Satoh T, Nishizawa O. The hierarchical rupture process of a fault: an
733 experimental study. *Phys Earth Planet In*. 2003; 137(1-4): 213-228.

734 24. Jeffieys H. A modification of Lomnitz's law of creep in rocks. *Geophys J Int*. 1958; 1(1): 92-
735 95.

736 25. Aydan O, Tokashiki N, Ito T, Akagi T, Ulusay R, Bilgin H. An experimental study on the
737 electrical potential of nonpiezoelectric geomaterials during fracturing and sliding. In:
738 *Proceedings of 10th ISRM Congress, International Society for Rock Mechanics*. South Africa;
739 2003: 73-78.

740 26. Penny R, Marriott D. *Design for creep*. Springer Science & Business Media; 1995.

741 27. Wang R, Li L. A non-stationary power law model to predict the secondary creep rate of rocks.
742 In: *Proceedings of 8th International Conference on Case Histories in Geotechnical*
743 *Engineering*. American Society of Civil Engineers (ASCE), Philadelphia, United States; 2019:
744 476-483.

28. Maruyama K, Tanaka C, Oikawa H. Long-term creep curve prediction based on the modified theta projection concept. *J press Vess-T ASME*. 1990; 112(1): 92-97.

29. Lockner DA. A generalized law for brittle deformation of Westerly granite. *J Geophys Res*. 1998; 103(B3): 5107-5123.

30. Mirza U. *Investigation into the design criteria for underground openings in rocks which exhibit rheological behaviour* (Ph.D. thesis). University of Newcastle upon Tyne; 1978.

31. Boukharov G, Chanda M, Boukharov N. The three processes of brittle crystalline rock creep. *Int J Rock Mech Min Sci*. 1995; 32(4): 325-335.

32. Fahimifar A, Karami M, Fahimifar A. Modifications to an elasto-visco-plastic constitutive model for prediction of creep deformation of rock samples. *Soils Found*. 2015; 55(6): 1364-1371.

33. Wang R, Li L. Burgers creep model used for describing and predicting the creep behaviour of a rock under uniaxial and triaxial compression test conditions. In: *Proceedings of the 71st Canadian Geotechnical Conference*. Edmonton, Canada; 2018: 572.

34. Lo KY, Yuen CMK. Design of tunnel lining in rock for long-term time effects. *Can Geotech J*. 1981; 18(1): 24–39.

35. Tomanovic Z. Rheological model of soft rock creep based on the tests on marl. *Mech Time-Depend Mater*. 2006; *10*(2): 135-154.

36. Xu M, Jin D, Song E, Shen D. (2018). A rheological model to simulate the shear creep behavior of rockfills considering the influence of stress states. *Acta Geotech*. 2018; 13(6): 1313-1327.

37. Andrade ENdC. On the viscous flow in metals, and allied phenomena. In: *Proceedings of the Royal Society of London*. Series A, The Royal Society; 1910: 1-12.

38. Garofalo F. *Fundamentals of creep and creep-rupture in metals*. Macmillan; 1965.

39. Lomnitz C. Linear dissipation in solids. *J Appl Phys*. 1957; 28(2): 201-205.

40. Jaeger JC, Cook NGW, Zimmerman R. *Fundamentals of rock mechanics*. John Wiley & Sons; 2009.

41. Paraskevopoulou C. *Time-dependency of rocks and implications associated with tunneling* (Ph.D. thesis). Queen's University; 2016.

42. Ito H. On rheological behaviour of in situ rock based on long-term creep experiments. In: *Proceedings of 7th ISRM Congress*. Aachen, Germany; 1991: (1) 265-268.

43. Nopola J, Roberts L. Time-dependent deformation of Pierre Shale as determined by long-duration creep tests. In: *Proceedings of 50th US Rock Mechanics/Geomechanics Symposium*, American Rock Mechanics Association; 2016: 584-591.

44. Bérest P, Béraud J, Gharbi H, Brouard B, DeVries K. A very slow creep test on an Avery Island salt sample. *Rock Mech Rock Eng*. 2015; 48(6): 2591-2602.

780 45. Maranini E, Yamaguchi T. A non-associated viscoplastic model for the behaviour of granite
781 in triaxial compression. *Mech Mater.* 2001; 33(5): 283-293.

782 46. Perzyna P. Fundamental problems in viscoplasticity. *Adv Appl Mech*. 1966; 9: 243-377.

783 47. Yahya O, Aubertin M, Julien M. A unified representation of the plasticity, creep and relaxation
784 behavior of rocksalt. *Int J Rock Mech Min Sci*. 2000; 37(5): 787-800.

785 48. Aubertin M, Gill D, Ladanyi B. An internal variable model for the creep of rock salt. *Rock*
786 *Mech Rock Eng*. 1991; 24(2): 81-97.

787 49. Shao J, Chau K, Feng X. Modeling of anisotropic damage and creep deformation in brittle
788 rocks. *Int J Rock Mech Min Sci*. 2006; 43(4): 582-592.

789 50. Tang H, Wang D, Huang R, Pei X, Chen W. A new rock creep model based on variable-order
790 fractional derivatives and continuum damage mechanics. *Bull Eng Geol Environ*. 2017; 77(1):
791 375-383.

792 51. Zhang H, Wang Z, Zheng Y, Duan P, Ding S. Study on tri-axial creep experiment and
793 constitutive relation of different rock salt. *Saf Sci*. 2012; *50*(4): 801-805.

794 52. Mansouri H, Ajalloeian R. Mechanical behavior of salt rock under uniaxial compression and
795 creep tests. *Int J Rock Mech Min Sci*. 2018; 110: 19-27.

796 53. Kemeny J. M. A model for non-linear rock deformation under compression due to sub-critical
797 crack growth. *Int J Rock Mech Min Sci*. 1991; 28: 459-467.

798 54. Miura K, Okui Y, Horii H. Micromechanics-based prediction of creep failure of hard rock for
799 long-term safety of high-level radioactive waste disposal system. *Mech Mater.* 2003; 35(3-6):
800 587-601.

801 55. Chandler NA, Martin CD. An analysis of laboratory and long-term rock strength using a
802 sliding crack model. In *Proceedings of the 35th US Symposium on Rock Mechanics (USRMS)*.
803 American Rock Mechanics Association; 1995: 741-747.

804 56. Myer LR, Kemeny JM, Zheng Z, Suarez R, Ewy RT, Cook NGW. Extensile cracking in porous
805 rock under differential compressive stress. *Appl Mech Rev*. 1992; 45(8): 263-280.

806 57. Freiman S. Effects of chemical environments on slow crack growth in glasses and ceramics. *J*
807 *Geophys Res*. 1984; 89(B6): 4072-4076.

808 58. Damjanac B, Fairhurst C. Evidence for a long-term strength threshold in crystalline rock. *Rock*
809 *Mech Rock Eng*. 2010; 43(5): 513-531.

810 59. Charles, R. The strength of silicate glasses and some crystalline oxides. In: *Proceedings of*
811 *International Conference on the Atomic Mechanisms of Fracture*. Swampscott, Massachusetts;
812 1959: 225–49.

813 60. Potyondy DO. Simulating stress corrosion with a bonded-particle model for rock. *Int J Rock*
814 *Mech Min Sci*. 2007; 44(5): 677-691.

61. Ladanyi B. Use of the long-term strength concept in the determination of ground pressure on tunnel linings. In: *Proceedings of the 3rd Congress of International Society of Rock Mechanics on Advances in Rock Mechanics*. Washington. National Academy of Science; 1974: (2)1150-1156.

62. Aubertin M, Li L, Simon R. A multiaxial stress criterion for short-and long-term strength of isotropic rock media. *Int J Rock Mech Min Sci*. 2000; 37(8): 1169-1193.

63. Diederichs M, Kaiser P, Eberhardt E. Damage initiation and propagation in hard rock during tunneling and the influence of near-face stress rotation. *Int J Rock Mech Min Sci*. 2004; 41(5): 785-812.

64. Li L, Aubertin M, Simon R. The $MSDP_u$ multiaxial criterion for the strength of rocks and rock masses. In: *Rock Mech & Eng*. CRC Press. 2017; 1: 409-436.

65. Brace W, Paulding Jr B, Scholz C. Dilatancy in the fracture of crystalline rocks. *J Geophys Res*. 1966; 71(16): 3939-3953.

66. Hallbauer D, Wagner H, Cook N. Some observations concerning the microscopic and mechanical behaviour of quartzite specimens in stiff, triaxial compression tests. *Int J Rock Mech Min Sci*. 1973; 10(6): 713-726.

67. Aydan O, Seiki T, Jeong G, Tokashiki N. Mechanical behaviour of rocks, discontinuities and rock masses. In: *Proceedings of International Symposium Pre-failure Deformation Characteristics of Geomaterials*. Sapporo; 1994: 1161-1168.

68. Martin CD. Seventeenth Canadian geotechnical colloquium: the effect of cohesion loss and stress path on brittle rock strength. *Can Geotech J*. 1997; 34(5): 698-725.

69. Gasc-Barbier M, Chanchole S, Bérest P. Creep behavior of Bure clayey rock. *Appl Clay Sci*. 2004; 26(1-4): 449-458.

70. Wang G, Zhang L, Zhang Y, Ding G. Experimental investigations of the creep–damage–rupture behaviour of rock salt. *Int J Rock Mech Min Sci*. 2014; 66: 181-187.

71. Charles R. Static fatigue of glass. I. *J Appl Phys*. 1958; 29(11): 1549-1553.

72. Kranz RL. The effects of confining pressure and stress difference on static fatigue of granite. *J Geophys Res*. 1980; 85(B4): 1854-1866.

73. Brantut N, Baud P, Heap M, Meredith P. Micromechanics of brittle creep in rocks. *J Geophys Res*. 2012; 117(B08412). doi:10.1029/2012JB009299.

74. Heap M, Baud P, Meredith P, Vinciguerra S, Bell A, Main I. Brittle creep in basalt and its application to time-dependent volcano deformation. *Earth Planet Sci Lett*. 2011; 307(1-2): 71-82.

75. Heap M, Baud P, Meredith P, Bell A, Main I. Time‐dependent brittle creep in Darley Dale sandstone. *J Geophys Res*. 2009; 114(B07203). doi:10.1029/2008JB006212.

76. Chin H, Rogers J. Creep parameters of rocks on an engineering scale. *Rock Mech Rock Eng*. 1987; 20(2): 137-146.

77. Das S, Scholz C. Theory of time-dependent rupture in the earth. *J Geophys Res*. 1981; 86(B7): 6039-6051.

78. Ashby M, Sammis C. The damage mechanics of brittle solids in compression. *Pure Appl Geophys*. 1990; 133(3): 489-521.

79. Li X, Qi C, Shao Z, Qu X. Static shear fracture influenced by historic stresses path and crack geometries in brittle solids. *Theor Appl Fract Mech.* 2018; 96: 64-71.

80. Julien MR, Foerch R, Aubertin M, Cailletaud G. Some aspects of the numerical implementation of SUVIC-D. In: *Proceedings of 4th Conference on the Mechanical Behavior of Salt*. Trans Tech Publications. Clausthal-Zellerfeld, Germany; 1998: 389-404.

81. Boulianne M, Simon R, Aubertin M. A numerical investigation of the creep (viscoplastic) behaviour of circular opening and pillar in rock salt. In: *Proceedings of 57th Canadian geotechnical conference and the 5th joint CGS-IAH conference*. Quebec City; 2004: 25-32.